

ARTICLE OPEN



Emergence of flexible kesterite solar cells: progress and perspectives

Jianjun Li¹✉, Kaiwen Sun¹✉, Xiaojie Yuan¹, Jialiang Huang¹✉, Martin A. Green¹ and Xiaojing Hao¹✉

Flexible photovoltaics have been and will be increasingly in demand in modern and future society in various applications. Searching for ideal flexible photovoltaic technologies that can perfectly meet these expanding demands has long been an active branch of photovoltaic research. Flexible kesterite $\text{Cu}_2\text{ZnSn}(\text{S},\text{Se})_4$ (CZTSSe) has emerged in recent years owing to its great potential to be an abundant, low-cost, stable, and high-efficiency 'green' photovoltaic material that can be widely deployed with the lowest detrimental environmental impact. Here, we review the recent progress with flexible kesterite solar cells in thin-film and monograin technologies, discuss the key challenges and strategies associated with the flexible substrates, and finally provide the future perspectives on further pushing the efficiency toward commercial-competitive levels.

npj Flexible Electronics (2023)7:16; <https://doi.org/10.1038/s41528-023-00250-7>

INTRODUCTION

Photovoltaics (PV) has been identified as one of the most important renewable sources, thanks to the historic achievements in the price reduction of crystalline-Si and CdTe-based PV technologies in the past decades¹. By far, most of the available PV products in the market are based on crystalline-Si solar cells and CdTe thin film solar cells, both encapsulated in rigid modules. Nevertheless, in the modern and future society, there are increasing opportunities for flexible photovoltaics (FPV) in various application scenarios, for instance, in building integrated photovoltaics (BIPV)², in-door photovoltaics³, power sources for the internet of things (IoT)⁴, space application⁵, and light-weight portable power sources⁶. FPV also has great advantages in roll-to-roll mass production, which enables significantly higher throughput, lower thermal budget, and more compact deposition equipment compared to batch-to-batch production of the rigid module technologies⁷.

Besides a high absorption coefficient that allows thin and flexible light absorber layer on flexible substrates, ideal FPV technology also requires materials with combined features of low-cost, long-term stability, eco-friendliness, high conversion efficiency, and excellent flexibility and reliability⁸. To date, such material perfectly meeting all these criteria is yet to be discovered or developed. Current commercialized FPV technologies are mainly flexible ultra-thin crystalline Si solar cells⁹, thin-film Si tandem solar cells¹⁰, flexible chalcopyrite $\text{CuInGa}(\text{S},\text{Se})_2$ (CIGSSe) thin-film solar cell and organic solar cells^{11,12}. Flexible III-V solar cells, though having very high power conversion efficiency (PCE), are only used for space and military applications due to their extremely high manufacture cost¹. The flexible crystalline Si solar cells still have issues about the fragileness. The commercialization of thin-film Si tandem and CIGSSe have stagnated in recent years owing to the relatively high manufacturing cost¹, whilst the commercialization of organic solar cells is limited by its relatively low module efficiency with additional concern of unsatisfactory long-term stability^{13,14}. Therefore, searching for alternative FPV technologies is still a hot topic in the field of photovoltaics.

In the recent years, kesterite $\text{Cu}_2\text{ZnSn}(\text{S},\text{Se})_4$ (CZTSSe)-based FPV has drawn increasing interest. CZTSSe stands at the front among the emerging inorganic photovoltaic materials, enjoying its earth abundant and environmentally friendly constituents, appropriate bandgap (1.0–1.5 eV) with high light absorption coefficients ($>10^4 \text{ cm}^{-1}$), and thermodynamically stable adamantine structure which also endows the quasi-three dimensional symmetric carrier transport that is important for efficient photovoltaic devices^{6,15–17}. The outdoor stability test performed by IMRA has shown that CZTSSe thin-film solar cells has negligible degradation in three and a half months field operation if well encapsulated¹⁸. Their other illumination tests on unencapsulated device also indicate that CZTSSe thin-film solar cells are quite promising in long-term stability¹⁸. The cost analysis performed by Wang et al.¹⁹ has indicated that CZTSSe thin-film technology has great advantage over CIGS thin-film technology in terms of manufacturing cost because of the abundant raw materials used¹⁹. This advantage is even larger when cheaper substrates such as flexible stainless steel are used¹⁹.

In the market potential analysis, there is a large gap for CZTS to entry the market that is dominated by crystalline silicon such as traditional rooftop, especially considering the efficiency of CZTS solar cells is still far from competitive. However, CZTS solar cells still foresee some niche deployment such as membrane roofs, Internet of Things (IoT) devices that demand low-weight and flexibility. Provided that the efficiency of CZTS solar cells can be enhanced to a more commercially acceptable level ($>15\%$), the commercialization pathway will become clearer. On the other hand, as the urge to develop high-efficiency and low-cost tandem PV technologies is more and more appreciated^{20–22}, flexible low bandgap CZTSSe has a great opportunity to be integrated into all-thin-film flexible tandem technologies as one of the few promising low-cost thin-film bottom cells²⁰. Low bandgap CZTSSe, especially pure-selenide CZTSe, has an optimal bandgap of $\sim 1.0 \text{ eV}$ for the bottom cell of a two-junction tandem^{23,24}. Moreover, the demerit of low-efficiency of CZTSSe could be largely mitigated, for instance, the efficiency gap between single junction CZTSSe and CuInSe_2 could be

¹Australian Centre for Advanced Photovoltaics, School of Photovoltaic and Renewable Energy Engineering, University of New South Wales, Sydney, NSW 2052, Australia.

✉email: jianjun.li@unsw.edu.au; kaiwen.sun@unsw.edu.au; xj.hao@unsw.edu.au

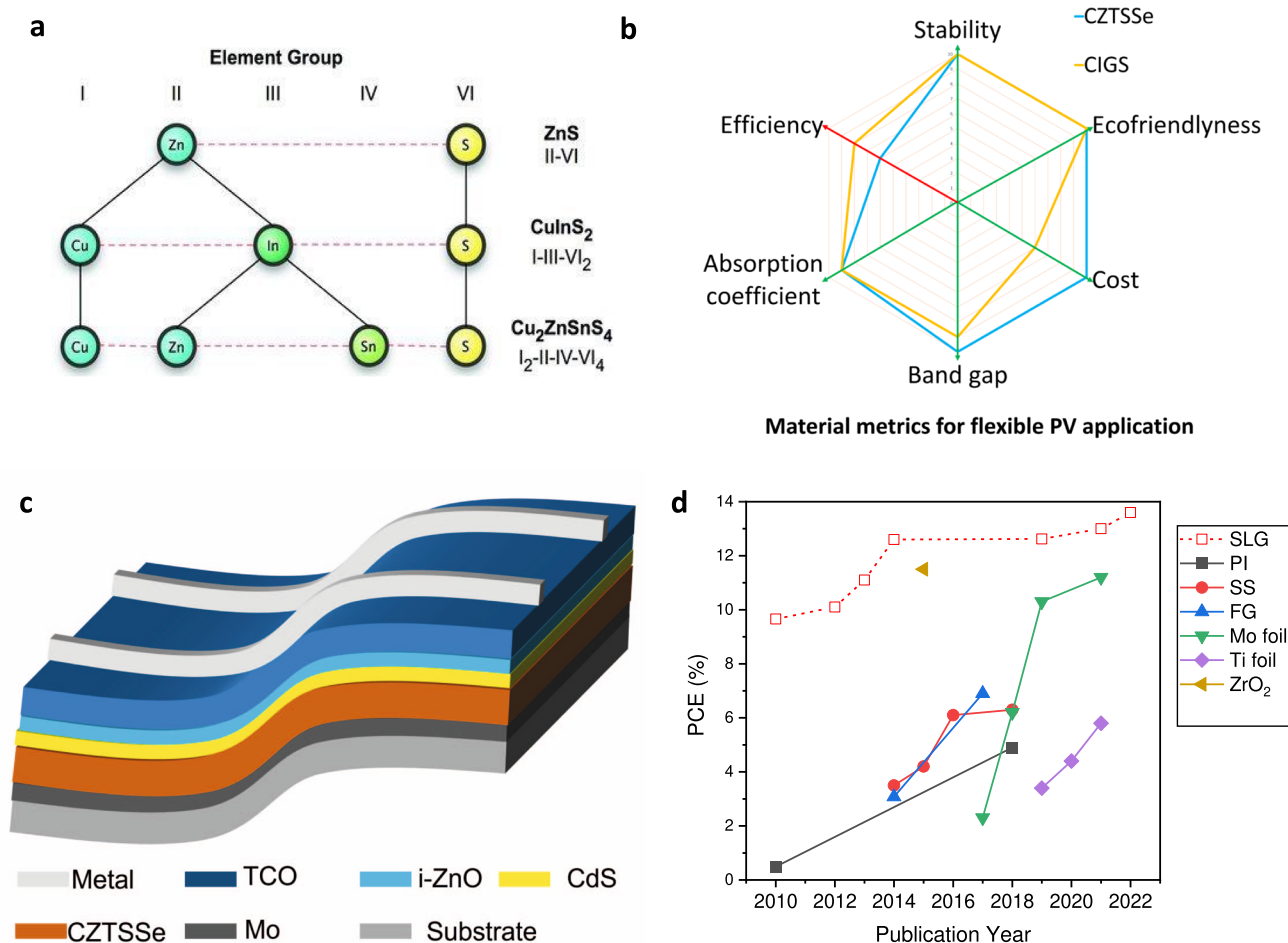


Fig. 1 Materials and device structure of flexible CZTSSe thin-film solar cells. **a** the thermodynamically favorable kesterite structure of CZTSSe. Reproduced with permission¹⁶. Copyright 2012, Wiley-VCH. **b** Material metrics of CZTSSe and CIGS for flexible PV application. **c** Schematic diagram of the typical device structure of flexible CZTSSe thin-film solar cells. **d** Evolution of record efficiencies of CZTSSe thin-film solar cells fabricated on various flexible substrates and on soda lime glass (SLG). (PI polyimide, SS stainless steel, FG flexible glass) The data are picked up from Table 1.

reduced by half if introduced into two-junction tandem as the bottom cells.

In principle, the upper limit power conversion efficiency of CZTSSe can be comparable to those of CIGS and CdTe which are believed to be well beyond 25% efficiency¹. However, the current efficiency of CZTSSe solar cells largely lags behind due to its relatively early stage of development against its unprecedented complexity, particularly in controlling secondary phases and intrinsic lattice defects^{15,25}. It is noteworthy that even remaining the large population of lattice defects and a low carrier lifetime of 0.1 ns, the upper limit of CZTSSe solar cells is still estimated to be >20%²⁶. The encouraging results in material and device characterization have shown that the intra-grain lifetime of CZTSSe in current state-of-the-art thin film solar cells can be larger than 10 ns, and the efficiency of CZTSSe thin-film solar cells can catch up CIGS and CdTe thin-film solar cells if the grain boundaries of CZTSSe thin films can be passivated to a similar degree to that of CIGS and CdTe²⁷. Furthermore, theoretically, if no bending applied, there should be no significant efficiency gap between the CZTSSe solar cells fabricated using flexible and rigid substrates respectively when suitable flexible substrates are available. Indeed, since the first flexible kesterite solar cell was made on polyimide (PI) substrate in 2010, the efficiency gap between flexible and rigid solar cells has been greatly reduced in recent years, although there are relatively limited research groups

working on flexible kesterite solar cells. Nevertheless, there are still outstanding issues for kesterite solar cells fabricated on flexible substrates, especially the management of the thermo-induced strain and the diffusion of critical trace elements related to substrates.

In this paper, we review the recent progress on the flexible kesterite cells and the specific technical challenges associated with the flexible substrates. A number of flexible substrates and kesterite thin-film deposition methods are compared and discussed; and some possible issues that may lead to the main efficiency deficit compared to the cells fabricated on glass substrates are discussed, providing a grasp of the key challenges and perspectives for the further development of flexible kesterite solar cells.

PROGRESS OF FLEXIBLE KESTERITE SOLAR CELLS

Kesterite CZTSSe inherits a similar material structure from chalcopyrite CIGS (Fig. 1a), which can be related to each other through the cross-substitution cation mutation¹⁶. For flexible PV applications, six metrics are usually considered to evaluate the light-active materials, which include sufficient stability, eco-friendliness, low manufacturing cost, band gap matching with the solar spectrum, high absorption coefficient enabling thin flexible absorber, and high power conversion efficiency (Fig. 1b).

CZTSSe possesses most of the above merits, except that the efficiency is currently much lower than CIGS, although there is still a large efficiency potential in CZTSSe to be exploited. Kesterite CZTSSe can be extended to a large material family through isovalent cation substitution and alloying, which provides more flexibility in tunability of bandgap and other optoelectronic properties. Except for Ag based kesterite, most of the CZTSSe family share similar charge carrier polarity with CIGS—suitable p-type doping (10^{15} – 10^{17} cm⁻³) for solar cell absorbers under Cu-poor condition^{16,28,29}. This means that the typical device architecture of CIGS solar cells can be directly copied to CZTSSe, and this has underpinned the fast efficiency development to >12% at the early developmental stage of low bandgap CZTSSe solar cells ($E_g=1.0$ – 1.2 eV)^{30,31}. Given that the elaborate engineering of the heterojunction interface is the foremost concern for device performance^{29,32,33}, to date, most CZTSSe solar cells are fabricated with superstrate architecture, typically, substrate/Mo/CZTSSe/CdS/i-ZnO/TCO/metal grid. This device architecture also applies for solar cells fabricated on flexible substrates. On the other hand, besides typical flexible solar cells fabricated with polycrystalline thin-film CZTSSe absorber, there are also flexible CZTSSe solar cells fabricated with monograin layer absorber³⁴. There are large technique differences between the fabrication processes of these two types of flexible CZTSSe solar cells, thus they will be discussed separately in the following.

Flexible thin-film kesterite solar cells

As shown in Fig. 1c, flexible thin-film CZTSSe solar cells usually take a device structure of substrate/Mo/CZTSSe/CdS/i-ZnO/TCO/metal grid. The Mo back contact can be omitted if Mo foil is applied as the substrate. It is well accepted that high quality CZTSSe thin-film absorber layer can only be fabricated under the protection of high inert gas pressure (Ar or N₂) during the high temperature annealing for grain growth^{30,35–40}, given that the surface decomposition of CZTSSe and the Sn loss due to volatile Sn(S,Se)_x at high temperature are detrimental to device performance^{41–43}. So, the current CZTSSe deposition approaches producing high efficiency solar cells share a mutual two-step process: precursors are made at low temperature using no matter vacuum or nonvacuum deposition processes to enable better control of the overall chemical composition; high temperature annealing for sufficient chalcogenization and grain growth is performed under the protection of high-pressure inert gas (Ar or N₂). At the current stage, CZTSSe solar cells are rather forgiving to precursor deposition technologies as they are to various doping alloying elements^{15,17,44}, while the conditions for high temperature annealing are more critical. Over 11% efficiency CZTSSe solar cells have been reported using solution-based precursor deposition approaches applying various solvents^{30,37,45–49}, and using vacuum-based approaches (sputtering or evaporation) with pure metal stacks or compound source materials^{35,36,39,50–54}. There are varieties of flexible substrates literally compatible with all these deposition approaches. They can be metal foils like stainless steel (SS), Mo foils, and Ti foils; ceramic foils like ZrO₂ and flexible glasses (FG); and some plastic foils like polyimide (PI).

The efficiency evolution of flexible CZTSSe solar cells on different substrates is summarized in Fig. 1d, along with that of the CZTSSe solar cells based on soda lime glass (SLG). More details about the flexible cells are listed in Table 1. The first flexible CZTSSe solar cells was fabricated on Polyimide (PI) substrate in 2010 by screen printing CZTS nanoparticles⁵⁵. The particle size of CZTS was only 30–50 nm and the efficiency was quite low (0.49%). Since then, there was little progress on flexible CZTS solar cells on PI substrate due to the strict processing temperature limitation of PI (<500 °C) until in 2018 the group from Catalonia Institute for Energy Research (IREC) reported a 4.9% efficiency CZTSe solar cells on such PI substrate⁵⁶. They used sputtered metal precursor and a

low temperature post-selenization annealing (450–490 °C). The detrimental SnSe₂ secondary phases were found in all the samples, which is a major performance loss mechanism apart from the reduced grain size⁵⁶. This indicates that a modified CZTSSe growth mechanism that enables better control of secondary phases and grain size at relatively low temperature is critical for the flexible CZTSSe solar cells on PI substrate. From 2014 to 2018, flexible CZTSSe solar cells on stainless steel (SS) substrate were reported by Midsummer⁵⁷, IREC^{58,59}, and UNSW group⁶⁰, with the highest efficiency of 6.3% achieved by UNSW. For CZTSSe solar cells on SS substrate, an elaborate impurity diffusion barrier and a sodium incorporation process are required. The typical diffusion barrier materials are sputtered Cr or Ti thin films, both of which are proven effective in controlling impurities for SS-based high-efficiency CIGS solar cells⁷. However, the current efficiencies achieved on SS substrate are much lower than that on SLG substrate. It is found that the grain size on SS substrate is usually smaller than that on SLG substrate even though the annealing temperature was nominally the same⁶⁰. The actual substrate temperature could be very different, thus leading to different grain size and material quality. On the other hand, the results from IREC group has shown that the diffusion of Cr and Fe from SS substrates is detrimental to the device performance⁵⁹. CZTSSe solar cells fabricated on flexible glass (FG, Corning willow Glass) substrates were reported using sputtered metal precursors and nanoparticle precursors by the groups from State University of New York and Purdue University, achieving 3.1% and 6.9% efficiencies, respectively^{61,62}. There are also reports on flexible CZTSSe solar cells fabricated on Ti foils since 2019, with efficiencies increasing from 3.4% to 5.8%^{63–65}.

Flexible CZTSSe solar cells on Mo foils are attracting considerable interest in recent years. Although the initial efficiency of CZTSSe solar cell on Mo foils was only 2.3%, demonstrated by the group from Fuzhou University in 2017⁶⁶, many research groups from Korea and China have joined this direction since then, fostering the rapid development in this direction. Using Mo foil as substrate, the traditional Mo back contact deposition process can be omitted. Given that the dominant impurities in Mo foil are S and Cu, both of which are benign to CZTSSe, no additional impurity diffusion barrier is required. Mo foil is also compatible with various precursor deposition processes, such as sputtering, spin-coating, and doctor-blading, achieving 11.2%⁶⁷, 10.2%⁶⁸, and 9.6%⁶⁹ efficiencies respectively with the incorporation of sodium. The 11.2% efficiency is achieved by DGIST. The open circuit voltage (V_{oc}) is comparable to their 12.6% efficient glass substrate champion cell, whilst the short circuit current density (J_{sc}) and the fill factor (FF) are lower, which may be attributed to the unfavorable carrier transport at the back contact—a lot of voids and ZnSe secondary phase can be found at the bottom of the absorber^{67,70}. It is noteworthy that DGIST also achieved 8.6% efficiency on 2.2 cm² Mo foil cells⁷¹. The large area uniformity is significantly improved and the detrimental defects are reduced by employing multilayer sputtered precursors (Fig. 2a–h)⁷¹. Bifacial flexible CZTSSe solar cells have been developed by the group from Fuzhou University using the spin-coating method, with both sides showing >9% efficiencies (Fig. 2i–o)⁷². This is enabled since the set-up of their selenization furnace can provide adequate heating and Se partial pressure for both the front and back side of the sample. They have also demonstrated that the flexible CZTSSe solar cells can deliver promising performance under in-door applications. Recently, Lin et al. from Sun Ya-Sen University demonstrated a 9.6% efficiency on Mo-foil-based flexible CZTSSe solar cells using doctor-blading—a more upscalable non-vacuum approach⁶⁹. This efficiency is realized by an elaborate sodium doping process, which will be discussed with other sodium doping strategies in the “Na incorporation” section.

Surprisingly, the highest reported efficiency of flexible CZTSSe thin-film solar cell, was achieved on a ZrO₂ sheet in 2015 by the

Table 1. Efficiency summary table of flexible CZTSSe thin-film solar cells on different substrates along with the record-level CZTSSe thin-film solar cells fabricated on SLG substrates.

Substrate	Device structure	Year	V_{oc} (mV)	J_{sc} (mA/cm ²)	FF (%)	η (%)	Institute	Note	Ref.
SLG	SLG/Mo/CZTSSe/CdS/i-ZnO/ITO/MgF ₂	2014	513	35.2	69.8	12.6	IBM	Spin coating	30
SLG	SLG/Mo/CZTS/CdS/i-ZnO/ITO/MgF ₂	2018	731	21.7	69.3	11.0	UNSW	Sputtering compound precursor	39
SLG	SLG/Mo/CZTSSe/CdS/i-ZnO/ITO/MgF ₂	2019	541	35.4	65.9	12.6	DGIST	Sputtering metal precursor	35
SLG	SLG/Mo/CZTSe/CdS/i-ZnO/AZO/MgF ₂	2020	491	37.4	68.2	12.5	UNSW	Sputtering metal precursor	36
SLG	SLG/Mo/CZTSSe/CdS/i-ZnO/ITO/MgF ₂	2021	529	33.6	72.9	13.0	NJUPT	Spin coating	113
SLG	SLG/Mo/CZTSSe/CdS/i-ZnO/ITO/MgF ₂	2022	538	36.2	69.8	13.6	IOP, CAS	Spin coating	114
PI	PI/Mo/CZTS/CdS/AZO	2010	386	4.8	27.0	0.49	Shanghai Jiaotong University	Screen printing	55
PI	PI/Mo/CZTSSe/CdS/i-ZnO/ITO	2018	337	27.2	53.2	4.9	IREC	Sputtering metal precursor, NaF +Ge doping	56
Al foil	Al foil/Mo/CZTS/ZnS/i-ZnO/ITO	2012	484	8.91	45.1	1.94	Donghua University	Nanocrystal-based ink	115
SS	SS/Cr/Mo/ZnO/CZTSSe/CdS/i-ZnO/AZO	2014	302	24.7	47.1	3.5	IREC	Sputtering metal precursor	58
SS	SS/DB/Mo-Na/Mo/CZTS/In ₂ S ₃ /i-ZnO/ITO	2015	531	13.9	50.8	4.2	Midsummer AB	Sputtering quaternary target	57
SS	SS/Cr/Mo/Mo-Na/Mo/ZnO/CZTSSe/CdS/i-ZnO/ITO	2016	360	29.7	56.8	6.1	IREC	Sputtering metal precursor, Ge doping	59
SS	SS/Ti/Mo/Mo-Na/Mo	2018	628	17.4	57.5	6.3	UNSW	Sputtering compound precursor	60
FG	FG/Mo/CZTS/CdS/i-ZnO/ITO	2014	491	10.6	59.2	3.08	State University of New York	Sputtering metal precursor	61
FG	FG/Mo/CZTSSe/CdS/i-ZnO/ITO	2017	370	31.7	58.4	6.9	Purdue University	Nanoparticle inks	62
Mo foil	Mo foil/CZTS/CdS/ZnO/AZO	2017	370	13.5	45.0	2.3	Fuzhou University	Sol-gel processed	66
Mo foil	Mo foil/CZTSSe/CdS/i-ZnO/ITO	2018	358	31.5	55.2	6.2	Fuzhou University	Spin-coating, Ag alloying	116
Mo foil	Mo foil/CZTSSe	2019	467	33.7	50.8	~8.0	Chonnam National University	Sputtering metal precursor	117
Mo foil	Mo foil/CZTSSe/CdS/ZnO/ITO	2019	390	30.0	57.7	6.8	Fuzhou University	Spin-coating	118
Mo foil	Mo foil/CZTSSe/CdS/i-ZnO/AZO	2019	513	35.2	57.2	10.3	DGIST	Sputtering metal precursor	71
Mo foil	Mo foil/CZTSSe/CdS/i-ZnO/ITO	2020	393	32.1	57.0	7.2	Fuzhou University	Spin-coating, Indium alloying	119
Mo foil	Mo foil/CZTSSe/CdS/i-ZnO/ITO	2021	436	33.8	63.2	9.3	Fuzhou University	Spin-coating, bi-facial	72
Mo foil	Mo foil/CZTSSe/CdS/i-ZnO/ITO	2021	505	34.6	50.8	8.9	Sun Yat-Sen University	Spin-coating	120
Mo foil	Mo foil/CZTSSe	2021	360	32.3	54.4	6.3	Henan University	Electrochemically deposited	121
Mo foil	Mo foil/CZTSSe/CdS/i-ZnO/AZO/ MgF ₂	2021	428	32.3	62.6	8.7	Ewha Womans University	Sputtering metal precursor	122
Mo foil	Mo foil/CZTSSe/CdS/ITO/ MgF ₂	2021	426	35.6	64.0	9.7	Fuzhou University	Spin-coating	123
Mo foil	Mo foil/Mo/CZTSSe/CdS/i-ZnO/AZO	2021	539	33.1	62.8	11.2	DGIST	Sputtering metal precursor, NaF	67
Mo foil	Mo foil/CZTSSe/CdS/i-ZnO/ITO	2021	483	35.4	56.2	9.6	Sun Yat-Sen University	Doctor-blading	69
Mo foil	Mo/CZTSSe/CdS/ZnO/ITO/Ag/MgF ₂	2022	463	35.6	62.5	10.2	Fuzhou University	Spin-coating	68
Ti foil	Ti foil/Mo/CZTSSe/ CdS/i-ZnO/ITO	2019	339	27.0	37.8	3.4	Nanjing University of Aeronautics and Astronautics	Sputtering	63
Ti foil	Ti foil/Mo/CZTSSe/ CdS/i-ZnO/ITO	2020	351	25.7	48.8	4.4	Nanjing University of Aeronautics and Astronautics	Sputtering	64
Ti foil	Ti/Mo/CZTS/CdS/ZnO/ITO	2021	609	20.8	46.0	5.8	Nanjing University of Aeronautics and Astronautics	Spin-coating	65
ZrO ₂	ZrO ₂ /Mo/CZTSSe/CdS/ZnO/ITO/Ni/Al/ MgF ₂	2015	452	38.4	66.1	11.5	IBM	Spin-coating	73

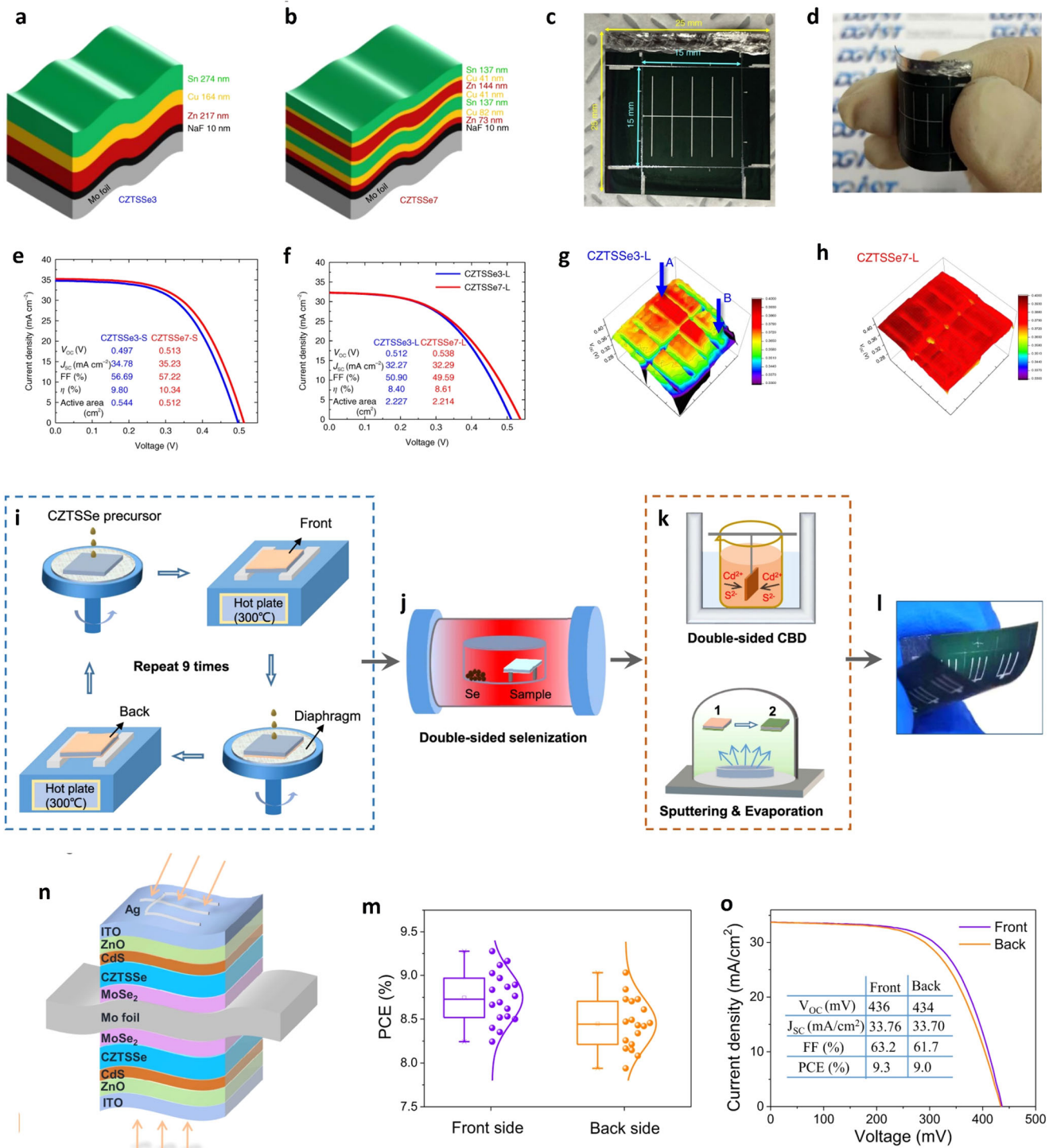


Fig. 2 Representative flexible CZTSSe thin-film solar cells fabricated on Mo foils. **a, b** 3-layer and 7-layer stacking structures respectively of the sputtered metal precursors on Mo foil substrates. **c, d** photos of a flexible CZTSSe cell with size of ~15 mm × 15 mm on a Mo foil substrate, fabricated by DGIST group. **e, f** Current–voltage curves of small area (~0.5 cm²) and large area (~2.2 cm²) flexible CZTSSe solar cells fabricated with 3-layer stacking precursor and 7-layer stacking precursor respectively. **g, h** Within-cell uniformity of V_{oc} measured by micro current–voltage for 2.2 cm² cells fabricated with 3-layer stacking precursor and 7-layer stacking precursor respectively. Reproduced with permission⁷¹. **i–l** Fabrication processes of solution-based bifacial flexible CZTSSe thin film solar cells on Mo foil substrates, developed by the Fuzhou University group. **n** Schematic diagram of the device structure of the bifacial flexible CZTSSe thin film solar cells. **m** Front and back side efficiencies of the bifacial CZTSSe thin-film solar cells. **o** Current density–voltage curves of the front cell and back cell of a representative bifacial CZTSSe cell. Reproduced with permission⁷².

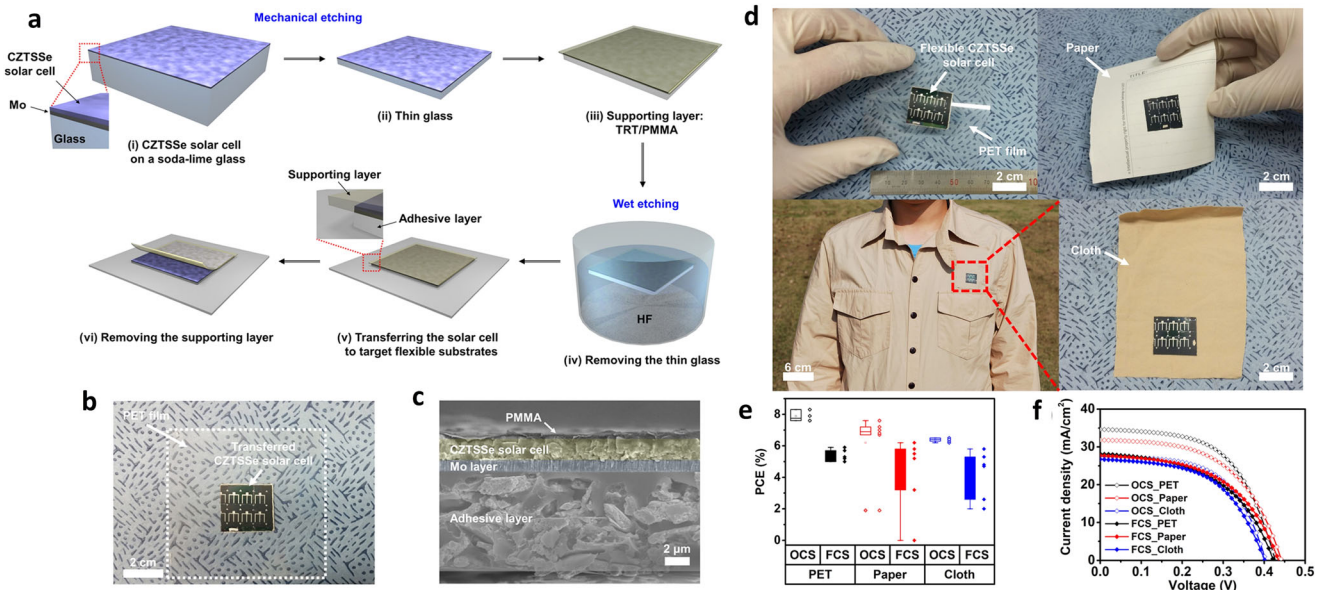


Fig. 3 Flexible CZTSSe thin-film solar cells based on substrate-transfer method. **a** The process flow of the substrate transfer method. **b** Photo of a CZTSSe thin-film sample transferred on to a PET substrate. **c** Cross-section SEM image of a transferred CZTSSe thin-film solar cell. **d** Photo demonstration of flexible CZTSSe thin-film solar cells transferred on PET, paper, and cloth substrates. **e, f** Efficiency and current density–voltage curves of the flexible CZTSSe thin-film solar cells transferred on different substrates respectively. Reproduced with permission⁷⁴. Copyright 2020, American Chemical Society.

IBM group. An 11.5% efficiency was achieved even though they encountered a significant bending issue during Mo sputtering and a uniformity issue during the solution precursor spin-coating⁷³. Though, this high efficiency should be partly attributed to their high efficiency baseline (12.6% on SLG substrate)³⁰, the results also indicate the high potential of ZrO₂ sheet as a flexible substrate. However, no follow-up research on ZrO₂ is reported, possibly due to the inadequate stiffness of this substrate resulting in difficulties in substrate handling for batch-to-batch R&D.

On the other hand, flexible CZTSSe thin-film solar cells on diverse flexible substrates have also been reported via an adhesive-bonding transfer method (Fig. 3). By using this method, the flexible CZTSSe thin-film solar cells can be transferred to various flexible substrates, such as poly (ethylene terephthalate) (PET), paper, and cloth as demonstrated⁷⁴. There are some damages to the cells during the transfer process and the highest efficiency ratio of the cells after and before transfer is around 0.91 with the best efficiency of 7.1% demonstrated on a PET substrate. There is a lot to explore about this interesting transfer method, for instance, how to improve the success rate and reduce the damage, how to realize monolithic series connection for modules, etc.

Flexible monograin layer kesterite solar cells

Flexible CZTSSe solar cells can also be made using monograin layer as light absorber. The monograin layer is a monolayer of CZTSSe grains embedded in an organic resin. The CZTSSe monograins can be single-crystals or grains composed of several single crystals, usually with a size of 30–100 μm, which are synthesized in a vacuum-sealed ampoule using binary compounds and elemental chalcogenides (S and Se) as raw materials and using molten salt KI as the fluxing agent to accelerate the solid-state reactions for the formation of CZTSSe monograins³⁴.

The fabrication processes of flexible monograin layer CZTSSe solar cells and the device structure are shown in Fig. 4a, b respectively. After CdS and transparent conductive oxide (TCO) layers are deposited on the monograin layer, the stacked layers are glued to a flexible transparent membrane^{75,76}. The back contact interface forms by attaching a graphite layer to the

plasma-etched monograin surfaces⁷⁵. Because the high-temperature synthesis of CZTSSe is a separate step and the processing temperatures for other layers are quite low (< 200 °C), the monograin layer CZTSSe solar cells can be intrinsically compatible with diverse transparent substrates like most polymer membranes. The separation of CZTSSe material synthesis from device and module fabrication also allows low-cost manufacture, controllable large-area homogeneity, and easy fitting into roll-to-roll production. Exploiting these advantages, CZTSSe monograin layer solar cells have already realized commercialization by the Tallin University of Technology spin-off company Crystalsol, which provides customer products that can be tailor made in shape, size, encapsulation substrates, and even in transparency¹⁸. Their semitransparent flexible products has more 5% power conversion efficiency¹⁸.

Due to the surface decomposition under high annealing temperature (> 700 °C) during the growth of monograins and the fast cooling down (~5 min from >700 °C to room temperature), the quality of the surface of the monograins is usually very poor and the bulk of monograins is disordered. Therefore, surface chemical treatments are critical for achieving high-efficiency monograin layer CZTSSe solar cells. Monograin powders are reported to be etched using 1% Br-MeOH followed by 10% KCN to remove the defective surface layer^{34,77}. An air annealing and surface CdS treatment are also found to further improve the quality of the CZTSSe monograins, particularly, making the monograins more ordered (Fig. 5a–d)⁷⁸.

Each monograin covered with buffer material is a unit solar cell in the monograin layer solar cells, and the entire monolayer solar cell can be regarded as a parallel integration of these miniature unit cells. Therefore, the power conversion efficiency is mainly determined by the performance of the monograin unit cells and how compact the unit cells are integrated—the inner interface of polycrystalline thin film (grain boundaries) and the large area homogeneity are no longer a concern. After removing the defective surface layer by chemical etching, and ordering treatment and surface passivation by air annealing, the efficiency of the monograin CZTSSe unit cell is estimated to be ~12%⁷⁹. While, due to the non-active area between the monograins, the

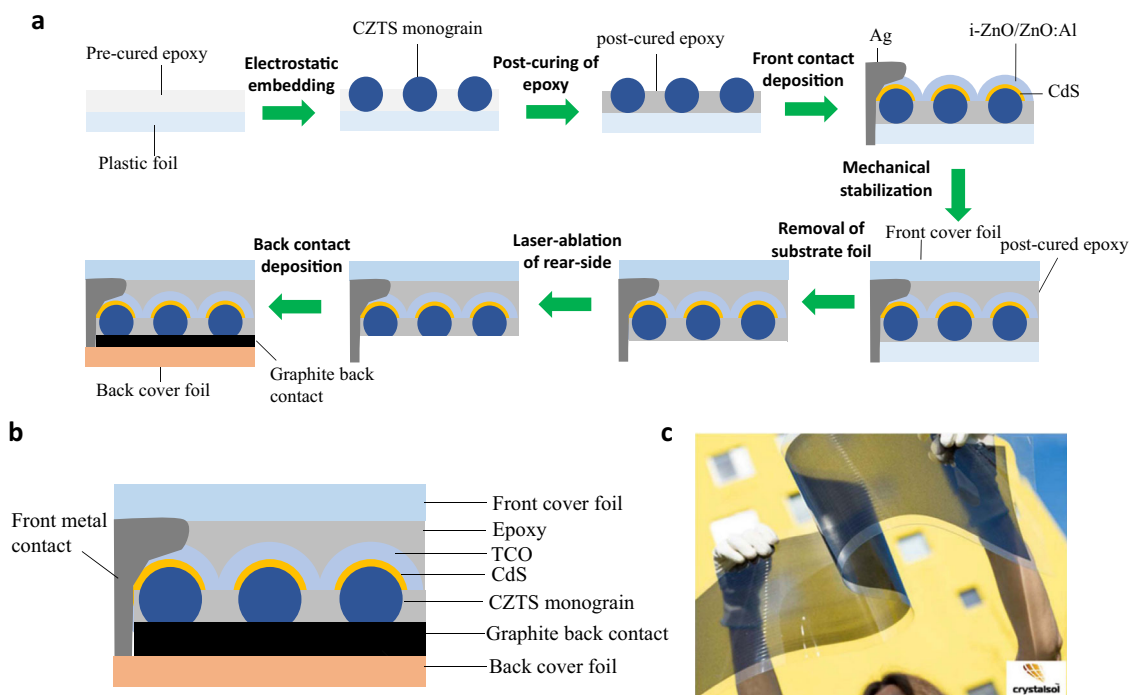


Fig. 4 flexible monograin layer CZTSSe solar cells. **a** Process flow to fabricate flexible monograin layer CZTSSe solar cells. **b** Schematic of the architecture of flexible monograin layer CZTSSe solar cells. **c** Photo demonstration of an endless flexible monograin layer CZTSSe module fabricated by CystalSol. Reproduced with permission¹⁸.

overall efficiency of monograin layer CZTSSe solar cells is slightly lower than the unit cells^{18,78,80,81}.

One would expect that the optoelectronic quality of CZTSSe monograins should be much better than that of the CZTSSe thin films since CZTSSe monograins are synthesized at higher temperature and the grain size is 10–100 times larger. However, this is not guaranteed. Secondary phases such as CuSe, ZnSe still can be observed in CZTSe monograins, and the overall composition still needs to be off-stoichiometry ($\text{Cu}/(\text{Zn}+\text{Sn})\sim 0.9\text{--}0.95$ and $\text{Zn}/\text{Sn}\sim 1.05\text{--}1.10$) to make good solar cells, which defines that abundant antisites defects should exist in CZTSSe monograins as they do in CZTSSe thin films³⁴. This has been verified by the fact that the as grown CZTSSe monograins are disordered and the significant red-shifting of photoluminescence (PL) can be observed even after the ordering treatment⁷⁸. The recent advances in bulk defect engineering of CZTSSe have shown that the formation of the deep level bulk defects $\text{Sn}_{\text{Zn}}^{2+}$ is mostly related to how CZTSSe is synthesis at temperature below 400°C ³⁶. $\text{Sn}(\text{S},\text{S})_x$ secondary phase companied synthesis should be avoided and the favorable local chemical environment (slightly Cu-poor and Zn-rich composition and Sn with +4 valence states) is desired^{36,82}. Therefore, high annealing temperature and large grain size do not guarantee a high bulk quality. The grain interior bulk quality of CZTSSe can be compared using the metrics Urbach energy (E_u) which can be extracted from the tail of EQE curves. The E_u values of some representative high efficiency kesterite solar cells made from thin-film absorber and monograins are listed in Table 2 along with the photovoltaic performance parameters. As shown in Table 2 and Fig. 5e, the E_u of representative high-efficiency pure-sulfide CZTS monograin layer solar cells fabricated by Talin University of Technology (TUT) is in a range of 45–55 meV, much larger than the E_u observed in the record thin-film CZTS solar cells (32.1 meV). Although the more defective grain interior yet larger bulk volume must lead to more non-radiative recombination in the quasi-neutral region of monograin CZTS solar cells, the V_{OC} deficit against the Shockley–Queisser (SQ) limit of monograin CZTS and thin-film CZTS are very close. For pure-selenide CZTSe, the

monograin CZTSe fabricated by University of Delaware shows slightly larger E_u compared to the record thin-film CZTSe, but much higher V_{OC} and lower V_{OC} deficit than any reported thin-film CZTSe solar cells⁷⁷. These contradictions could be attributed to the difference in non-radiative recombination at grain boundaries of monograin and thin-film solar cells. Monograin solar cells have much less grain boundary recombination due to their much larger grain size, which in turn leads to more recombination in the quasi-neutral region. It has been unveiled that grain boundary recombination is dominating in high-efficiency pure-selenide CZTSe thin-film solar cells²⁷. Also it is highly likely that grain boundary recombination may play an important role in the carrier loss of both pure-sulfide CZTS and S-Se mixed CZTSSe thin-film solar cells. On the other hand, the fill factors (FF) of monograin kesterite solar cells are lower than those of the best thin-film solar cells, which may arise from the increase of bulk resistance due to the too thick absorber compared to the limited hole conductance.

KEY CHALLENGES OF FLEXIBLE KESTERITE SOLAR CELL

The current major challenge of kesterite solar cells is the power conversion efficiency, regardless of the technologies based on rigid or flexible substrates. Particularly, for monograin kesterite solar cells, the key challenges are mainly associated with the defects in the bulk of kesterite monograins and at the interfaces. These challenges need to be overcome by combining the efforts from the entire community, particularly by understanding more about the material and devices on the basis of advanced characterizations, first-principal calculations, and device modeling, and by integrating these understandings into critical material and device processing steps. Nevertheless, there are additional challenges that flexible thin-film kesterite solar cells face, which include flexibility and reliability under bending stress, control of impurity and thermal strain arising from the flexible substrates, and incorporation of alkali elements into the material growth. These are discussed separately in the following.

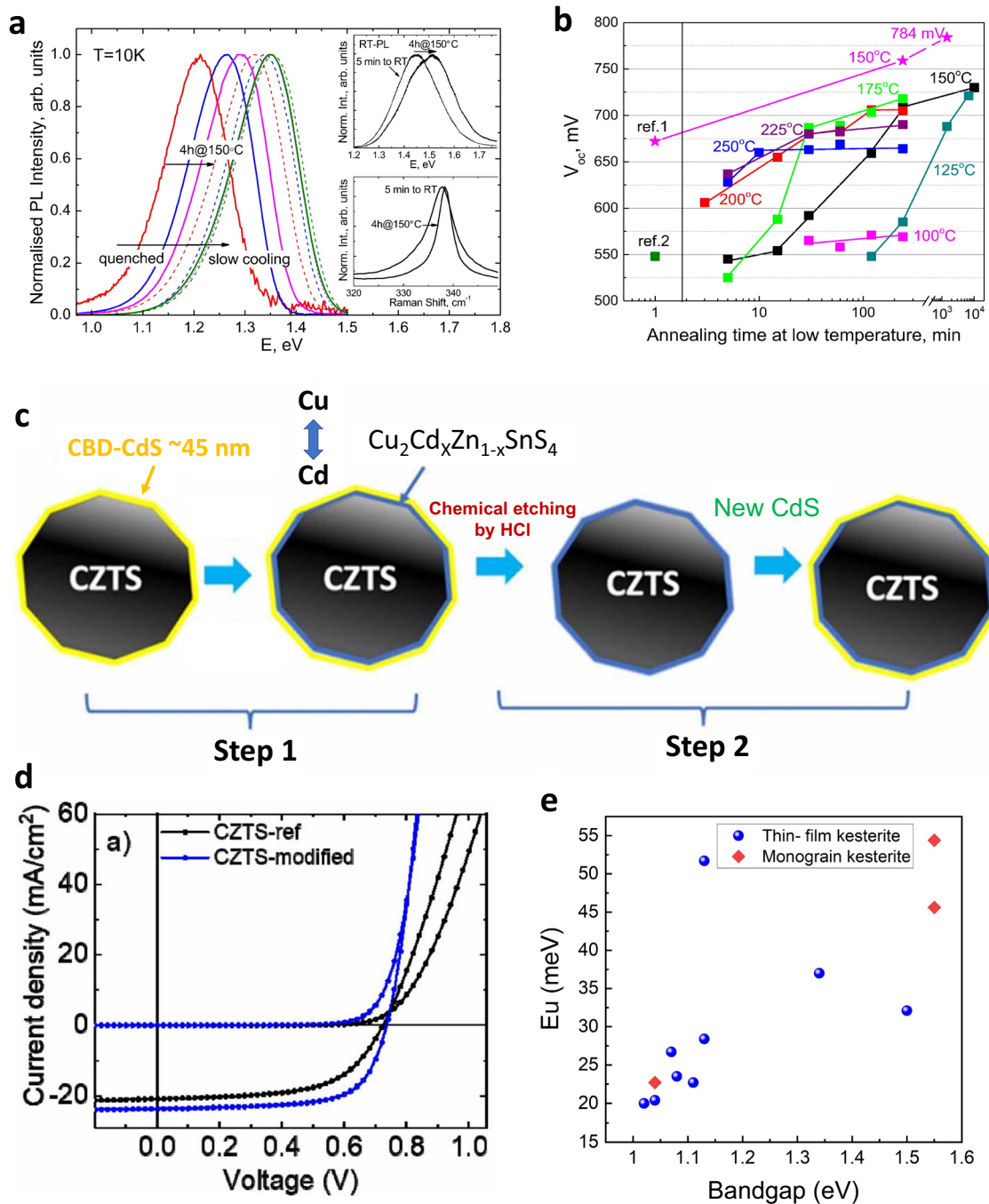


Fig. 5 Key post treatment steps for CZTSSe monograin solar cells and the device performance. **a, b** Evolution of photoluminescence (PL) and open circuit voltage (V_{oc}) of CZTS monograin layer solar cells after annealing at low temperature (ordering treatment), respectively. Reproduced with permission⁸⁰. Copyright 2016, Elsevier B.V. All rights reserved. **c** Processing steps of surface CdS treatment for CZTS monograin layer solar cells. **d** Dark and illuminated current density-voltage curves of the CZTS monograin layer solar cells with and without CdS surface treatment. Reproduced with permission⁸¹. **e** Plot of Urbach energy (E_u) against bandgap of representative CZTSSe monograin layer solar cells and thin-film solar cells. The values of E_u are listed in Table 2.

Flexibility and reliability

Flexibility is an important metric for flexible photovoltaic devices regarding their performance after bending cycling and/or under bending stress. Different application scenarios require different flexibility performance. For instance, BIPV applications require high performance under stationary bending stress, while wearable power sources require highly durable devices that can bear numerous bending cycles¹¹. Besides the flexibility of the substrate and encapsulation materials, the flexibility performance is also

determined by the robustness of the device structure under lateral compressive and/or tensile stress. Stress may lead to reversible changes (such as stress-induced bandgap changes, defect and doping changes in absorbers, buffer materials, and window layers) and irreversible changes such as inelastic deformations (cracks and delamination). The latter occurs when the applied stress or the bending cycles exceeds certain critical points, and it usually causes permanent degradation of device performance and accumulates after bending cycles. These critical

Table 2. Efficiency table of representative monograin layer CZTSSe solar cells and thin-film solar cells with different bandgaps.

Device	V_{oc} (mV)	J_{sc} (mA/cm ²)	FF (%)	PCE (%)	E_g (eV)	$V_{oc}/V_{oc,so}$ (%)	E_u (meV)	Institute	Ref.
CZTSSe	541	35.4	65.9	12.6	1.13	61.0	28.4	DGIST	35
CZTSSe	513	35.2	69.8	12.6	1.13	58.0	51.7	IBM	30
CZTSSe	547	34.3	70.0	13.1	1.11	63.0	22.7	IoP CAS	38
CZTSSe	485	37.5	64.9	11.8	1.07	58.5	26.7	CNU	124
ACZTSSe	540	32.1	72.3	12.5	1.08	64.2	23.5	NJUPT	37
CZTSe	491	37.4	68.2	12.5	1.04	61.4	20.4	UNSW	36
CZTSe	478	36.9	70.5	12.5	1.02	60.9	20.0	UNSW	27
CZCTS	640	27.8	71	12.6	1.34	59.1	37.0	ZSU	125
CZTS	731	21.7	69.3	11.0	1.50	59.4	32.1	UNSW	39
Monograin CZTS	759	19.0	63.0	9.1	1.55	59.3	45.6	TUT	80
Monograin CZTS	735	23.6	67.7	11.7	1.55	57.5	54.4	TUT	81
Monograin CZTSe	501	28.8	66.9	9.64	1.04	62.3	22.7	University of Delaware	77

The Urbach energies are extracted from EQE data to compare the bulk optoelectronic quality of the CZTSSe absorber layers.

points for irreversible changes are useful metrics to evaluate the flexibility and reliability of flexible photovoltaic devices. The critical point of stress can be evaluated using the minimum radius of curvature or the maximum bending angles the device can stand without significant degradation⁸³, while the critical point of bending cycles can be evaluated using the maximum bending cycle numbers in safe curvature radius⁸³.

Deng et al. have investigated the flexibility and reliability of CZTSSe thin-film solar cells fabricated on Mo foils⁷². As shown in Fig. 6a, b, the bending stress is modulated by changing the bending angle, and the responses to squashing (concave) bending and stretching (convex) bending were measured at the same time on their symmetrical bifacial devices. The results indicate that the maximum bending angle of their flexible CZTSSe solar cells is around 70°, and their devices can stand more concave bending cycles (more than 4000 cycles) than convex bending cycles (start to degrade at 2000 cycles) under a mild bending angle of 50°. They observed that the degradation is caused by the damaging of some absorber grains. Min et al. also investigated the flexibility of CZTSSe thin film solar cells on poly-ethylene terephthalate (PET) substrate via substrate transfer method⁷⁴. Their results indicate the CZTSSe thin film solar cells on PET have reliability up to a bending radius of 1.3 cm and 500 bending cycles⁷⁴. These flexibility and reliability test results are very encouraging for many applications. The above results indicate that the flexibility and reliability of flexible kesterite thin-film solar cells is mainly related to the substrate material and the absorber layers. However, based on the investigation performed on flexible CuInGaSe₂ thin film solar cells, the flexibility and reliability may be limited by the transmittance conductive oxides (TCO) electrode⁸³. As shown in Fig. 6e–g, devices based on indium doped tin oxide (ITO) show better flexibility and reliability than that based on ZnO:Al (AZO), whilst the devices based on sandwich electrode (AZO/Ag nanowires/AZO, AAA) show the best flexibility and reliability⁸³. By inserting metal nanowires, the flexibility and robustness of TCO electrode is significantly increased, thereby increasing the flexibility performance of devices.

However, there is very limited result about the performance of flexible CZTSSe solar cells under stationary bending conditions. This may be attributed to the lack of relevant measurement standards. It is difficult to estimate the power conversion efficiency of a solar cells under bending conditions because the cell is not uniformly illuminated, and the actual device area is also hard to define. Recently, Ha Kyung Park et al. have investigated the performance of flexible CZTSSe thin film solar cells under bending stress. As shown in Fig. 7, they used Kelvin Probe Force Microscopy (KPFM) to

measure the surface photovoltage (SPV) under concave and convex bending conditions. The results show a clear SPV decrease at grain boundaries under both concave and convex bending conditions compared to the planar condition, indicating an increased recombination under bending conditions. While in all the conditions, the addition of Na significantly increases the SPV. Their results also indicate the bandgap of CZTSSe absorber is slightly reduced under concave conditions and slightly increased under convex conditions. On the other hand, the direct comparison of photovoltaic performance under bending conditions is not available, and the change of stress induced defects is still unclear. These are important topics to be investigated for better understanding the performance of flexible kesterite solar cells under bending stress.

Thermal stress management and impurity control

One challenge the flexible CZTSSe thin-film solar cells encounters is the mismatch of coefficient of thermal expansion (CTE) between CZTSSe thin-film and the flexible substrates, which may raise risks of delamination and crack formation during the high temperature processing for CZTSSe formation. The values of CTE of the materials for device fabrication and the substrates are listed in Table 3, along with other typical property coefficients (maximum processing temperature, thickness, density, and possible impurities). The CTE of CZTSSe is between $9.9 \times 10^{-6} \text{K}^{-1}$ and $12 \times 10^{-6} \text{K}^{-1}$, similar to that of CIGS. Among the metal substrates, stainless steel and Ti have suitable CTE, while the CTEs of Cu, Al, mild steel are too large and the CTE of Mo is a bit small. The mismatch of CTE can be managed by inserting a CTE buffer layer which has intermediate CTE if the mismatch is not too large, or has loose structure so that the thermal stress can be relaxed within the buffer layer. The double layer structure of Mo contact represents a good example: the first Mo layer with loose structure deposited on substrate is used to relax the thermal stress at high annealing temperature while the second Mo layer with dense structure provides good electric conductivity⁸⁴. Interestingly, most of the CZTSSe thin-film absorbers have a loose fine grain layer at the bottom⁸⁵, especially for the solution-based fabrication process⁷². These fine grain layers can act as good CTE buffer layer, which may explain the good adhesion of flexible CZTSSe solar cells on various flexible substrates so far. However, large grain spanning thin-film absorbers are essential for higher power conversion efficiency and they are being achieved in both solution and vacuum-based approaches^{46,86}. The management of thermal stress in large grain spanning flexible CZTSSe absorber will need another CTE buffer layer such as a loss-structure Mo layer.

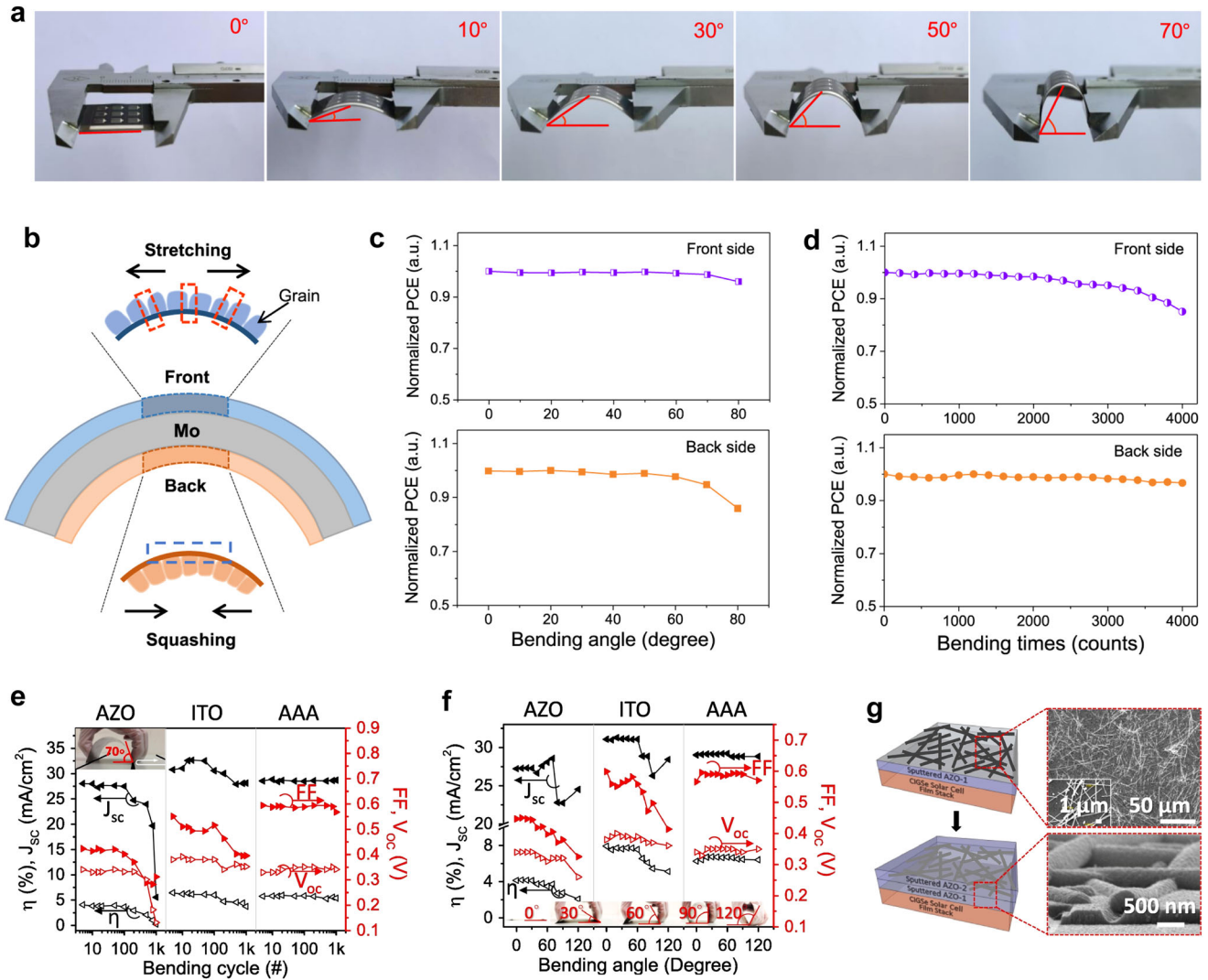


Fig. 6 Flexibility of CZTSSe thin-film solar cells. **a** Photographs of bended bifacial CZTSSe solar cells fabricated on Mo foils at varied angles from 0° to 70°. **b** Schematic bending states with stretching and squashing of front (convex) and back (concave) sides. **c** Normalized PCE degradation percent of bifacial solar cells at different bending angles (0°–80°) with 100 time bending. **d** Normalized PCE degradation evolution with different bending cycles (0–4000 times) at a fixed angle of 50°. Reproduced with permission⁷². **e, f** The bending test of AZO, ITO and AZO/Ag nano-wires/AZO (AAA) electrodes on flexible CIGS solar cells **e** with 1000 cycles and **f** different bending angles. **g** The schemes of fabrication of AAA transparent conductive electrodes. The insets show the top-view images of Ag nanowires on the 1st layer of AZO thin film and cross-section view image of AAA electrodes. Reproduced with permission⁸³. Copyright 2019, Elsevier B.V. All rights reserved.

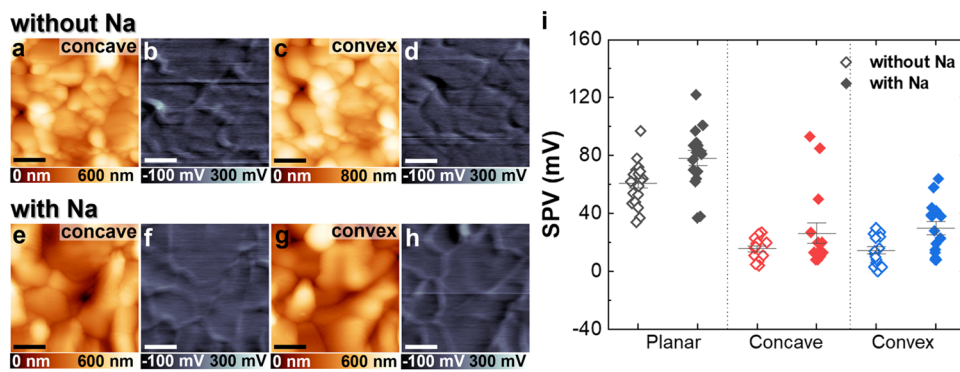


Fig. 7 Surface photovoltage (SPV) of CZTSSe flexible solar cells under different bending modes. **a–h** Surface topography (**a, c, e, g**) and local SPV variation map (**b, d, f, h**) of Na-undoped and doped CZTSSe in the concave and convex states. (scale bar: 1 μm) **i** Surface photovoltage (SPV) at GBs for CZTSSe with and without Na. Reproduced with permission¹¹².

Table 3. Typical properties of materials and substrates used for flexible CZTSSe thin-film solar cells.

Material	CTE (10^{-6}K^{-1})	Max. T ($^{\circ}\text{C}$)	Thickness (μm)	Density (g cm^{-3})	Possible impurities	References
CuInSe ₂	7–11		2–3	5.8		7
CZTS	12		0.8–1	4.5		126
CZTSe	9.9		1.5–2	5.0		127
Mo contact	5.35		0.5–1	10.2		
MoS ₂	1.9–8.6		0.05–0.2			128
MoSe ₂	7.2–12.9		0.05–0.5			128,129
ZnO	3–5		0.1–0.5	5.6		7
SLG	9	550–600	2000–5000	~2.5	Na, K, Ca	
Stainless steel	10–11	»600	30–200	8	Fe, Co, Ni,	
Mild steel	13	»600	25–200	7.9	Fe, Co, Ni,	
Cu	16.6	»600	50–100	8.9	Ca, Al, Si, Fe	
Ni/Fe alloys	5–11	»600		8.3	Ni, Fe, Co	
Ti	8.6	»600	25–100	4.5	Fe	
Mo	5.35	»600	100	10.2	W	
Al	23	600	100	2.7	Fe, Si, Mn	
ZrO ₂	5.7	»600	50–300	5.7	Zr	
PI	12–24	<500	12.5–75	1.4		7
PET	60	<500	300–400	1.4		7

Properties of CuInSe₂ and SLG are included for comparison.

For Polyimide (PI) and PET substrates with even larger CTE, more careful adaption of processing conditions is required.

The metal impurity in metal foil substrates is another issue for the related flexible CZTSSe thin-film solar cells. The possible metal impurities in different flexible substrates are summarized in Table 3. At current state, CZTSSe seems very forgiving to various metal impurities. The isovalent metal elements are theoretically predicted to be favourable or benign, like Ag⁸⁷, Cd⁸⁸, Ge^{26,40}, and some transition metal elements even like Mn, Ni, Co, Fe are reported to be benign to CZTSSe^{89–91}. However, this may be only valid when the baseline efficiency is relatively low, possibly because there are too many deep intrinsic defects dominating the recombination process in these solar cells. When the efficiency is improved to higher level, say the issue of intrinsic deep defects is addressed, the tolerance of impurities may be significantly reduced to a level that is comparable to CIGS. In that case, the impurities in substrates need to be carefully assessed. It is still unclear how sensitive CZTSSe is to these impurities so that impurity control will be increasingly important for high efficiency flexible CZTSSe solar cells. Impurity barrier layers such as Ti, SiO_x, SiN_x, Al₂O₃, AlN films that are typically used for high efficiency CIGS solar cells can also be applied to flexible CZTSSe solar cells^{7,92,93}. When these impurity barriers are embedded, the adaption of processing conditions for thermal stress management still needs to be considered.

Na incorporation

Alkali element incorporation is another critical issue that needs to be addressed in order to achieve high-efficiency flexible CZTSSe solar cells. Like in the case of CIGS, alkali element sodium (Na) and lithium (Li) play a key role in the synthesis of high quality CZTSSe thin films: not only facilitating the grain growth^{94,95}, but also significantly reducing the defects that act as non-radiative recombination centers^{94,96}, and increasing the effective p-type doping density (especially Li)^{97,98}. Although the detailed mechanisms are still under debate, it has been a consensus that Na seems a “must” in the synthesis of CZTSSe thin films for solar cells. For CZTSSe thin-film solar cells grown on SLG substrates, Na can

naturally diffuse from the SLG substrate and effectively incorporate into the growth of CZTSSe during high-temperature annealing, thus no elaborate Na incorporation control process is required at current stage. However, most of the flexible substrates are lack of Na and other alkali source. Therefore, in the flexible CZTSSe solar cells fabrication process, Na incorporation using external source become one of the key processing steps.

Na incorporation is usually directly fitted into the precursor deposition process. In the solution process, the Na source can be introduced into the solution or molecular ink and deposited together with the CZTSSe precursor film without requiring an additional step for Na elements incorporation^{59,99}, or it can be introduced by similar low-cost and simple solution post-treatment method⁶⁵. Researchers from Sun Yat-Sen University found that incorporating Na into the molecular ink for doctor-blading process for flexible CZTSSe solar cells could facilitate the grain growth, carrier transport, and defect passivation. With a novel blading strategy via coating Na-containing and Na-free molecular inks by turns to control the Na incorporation amount, they obtained compact and homogeneous CZTSSe films with large grains, and a flexible device with an efficiency of 9.63% on Mo foil⁶⁹.

In the vacuum-based process for CZTSSe absorbers, the Na is usually introduced by sputtering or evaporation methods to keep the fabrication processes compatible. Both IREC and UNSW investigated different vacuum-based methods for incorporating alkali in their flexible CZTSSe on SS substrates^{59,60,100}. They found that depositing appropriate thickness of NaF or KF layer below the CZTSSe precursor film or on top of the metal stack layers before high temperature annealing could effectively enhance the device performance comparing with the device without alkali element doping. Another promising route they reported is to source Na from Na-containing Mo back contact, which was realized by sputtering Na-doped Mo targets (Mo:Na) when preparing the back contact on top of the flexible substrates. They revealed that a Mo:Na layer (Na 5 at% or 10 at%) sandwiched between two Mo layers supplied sufficient Na into the CZTSSe absorber and contributed to remarkable efficiency improvement⁶⁰. Direct contact of CZTS and Mo:Na layer is not desirable because it caused poor adhesion and film delamination.

The Mo:Na layer incorporation route is favorable for industrial implementation since it can be easily integrated into the back contact sputtering step. DGIST also introduced Na into the CZTSSe absorbers by evaporating a 10 nm NaF before metal precursors deposition, which enabled the first over 10% flexible CZTSSe cell on Mo foil substrate⁷¹. They further systematically investigated the sodium doping effect on the CZTS properties by altering the position of the NaF within the metal stacks of the precursors⁶⁷. They revealed that the position of NaF in the precursors is important as it must be ensured that the NaF layer does not interfere the reaction path and the growth mechanism of CZTSSe, and meanwhile make sure that Na can be effectively incorporated to the entire absorber.

It is noteworthy that there are some reports demonstrated decent device performance nominally without introducing alkali elements into the system. For example, Fuzhou University achieved over 9% flexible CZTSSe solar cells on Mo foil using spin-coating method and they also demonstrated the symmetrical bifacial CZTSSe solar cell described earlier in this work⁷². After that, they recently further boosted the efficiency over to 10% by modifying the selenization process, still nominally without Na involving⁶⁸. However, they used SLG to support their flexible substrates during selenization process, which may unintentionally introduce trace amounts of Na into their CZTSSe samples. On the other hand, when carefully examining their CZTSSe absorbers in the high-performance devices, a thick fine grain layer under the top large grain layer cannot be avoided. Although the bi-layer structure is common in the solution-based process, it is likely that the thickness of fine grain layer can be reasonably reduced if sufficient Na can be incorporated to promote the grain growth.

OUTLOOK AND FUTURE PERSPECTIVES

As summarized above, flexible CZTSSe solar cells have attracted increasing attention and great progress has been made in recent years. Over 10% efficiency solar cells have been demonstrated on various flexible substrates using various deposition techniques. Monograin layer solar cell technology has pioneered the commercialization of CZTSSe solar cells. The efficiency gap between flexible and rigid CZTSSe thin-film solar cells arising from additional requirements on flexibility, thermal stress management, impurity control, and alkali incorporation is closing rapidly even though there are limited groups working on flexible CZTSSe.

The further development of flexible CZTSSe solar cells and their prospective commercialization depend on the progress of the entire CZTSSe field. Though the efficiency of CZTSSe solar cells is still not competitive in commercialization, substantial progress on fundamental understanding of the materials and device loss mechanisms has been made in recent years, particularly, in the advanced characterization technologies for the determination of secondary phases and electronic band alignment^{101–105}, the understanding of the killer defects in the bulk of CZTSSe and effective strategies to control the formation of these defects^{36,106–108}, the understanding of key role of isovalent cation and alkali doping/alloying¹⁰⁹, the understanding of the carrier loss mechanisms in the bulk, at junction interfaces, and at grain boundaries^{27,29,110}, and effective strategies to boost the carrier transport at front and back interfaces^{33,111}.

Based on our recent findings, if these critical understandings and strategies can be properly integrated, for instance, the lateral grain size can be larger than 3 μm while high grain interior quality (electron lifetime and hole density) can be maintained and the junction interface can be well passivated by an epitaxial ZnSe nano-layer, a step-change to 15% efficiency is highly possible²⁷. While further step-change in efficiency to 20% requires essential understanding of the grain boundaries of CZTSSe thin films and effective grain boundary passivation strategies²⁷. To achieve this

long-term goal, cation doping and/or alloying will also be important to get a high electron lifetime (50–100 ns) and suitable hole density ($\sim 5 \times 10^{16} \text{ cm}^{-3}$) simultaneously²⁷. As the issues of thermal stress management and impurity control can be properly addressed in principle using existing strategies on various flexible substrates and the alkali incorporation process can be further developed to near perfection, the efficiency of flexible CZTSSe thin-film solar cells will be on par with rigid CZTSSe solar cells. In other words, the important progress in the rigid CZTSSe thin-film solar cells can be easily transferred to the flexible CZTSSe solar cells, making both CZTSSe technologies more competitive in the future. Certainly, this requires closer and more intense collaboration and communication between the groups in the thin-film solar cell community to share and combine the understanding from the different perspectives of theoretical calculation, material processing, device physics, and characterizations.

DATA AVAILABILITY

The datasets analyzed and generated during the current study are included in the paper and its Supplementary Information.

CODE AVAILABILITY

The codes used for simulation within this paper are available from the corresponding author upon reasonable request.

Received: 22 September 2022; Accepted: 10 March 2023;

Published online: 23 March 2023

REFERENCES

1. Wilson, G. M. et al. The 2020 photovoltaic technologies roadmap. *J. Phys. D Appl. Phys.* **53**, 493001 (2020).
2. Arnaout, M. A., Go, Y. I. & Saqaff, A. Pilot study on building-integrated PV: technical assessment and economic analysis. *Int. J. Energy Res.* **44**, 9538–9559 (2020).
3. Li, M., Igbari, F., Wang, Z. K. & Liao, L. S. Indoor thin-film photovoltaics: progress and challenges. *Adv. Energy Mater.* **10**, 2000641 (2020).
4. Park, J., Joshi, H., Lee, H. G., Kiaei, S. & Ogras, U. Y. Flexible PV-cell modeling for energy harvesting in wearable IoT applications. *ACM Trans. Embed. Comput. Syst.* **16**, 1–20 (2017).
5. Ho-Baillie, A. W. Y. et al. Deployment opportunities for space photovoltaics and the prospects for perovskite solar cells. *Adv. Mater. Technol.* **7**, 2101059 (2022).
6. Liu, F. et al. Emerging inorganic compound thin film photovoltaic materials: progress, challenges and strategies. *Mater. Today* **41**, 120–142 (2020).
7. Reinhard, P. et al. Review of progress toward 20% efficiency flexible CIGS solar cells and manufacturing issues of solar modules. *IEEE J. Photovolt.* **3**, 572–580 (2012).
8. Wong, L. H. et al. Emerging inorganic solar cell efficiency tables (Version 1). *J. Phys. Energy* **1**, 032001 (2019).
9. Hwang, I. et al. Flexible crystalline silicon radial junction photovoltaics with vertically aligned tapered microwires. *Energy Environ. Sci.* **11**, 641–647 (2018).
10. Cashmore, J. S. et al. Improved conversion efficiencies of thin-film silicon tandem (MICROMORPH™) photovoltaic modules. *Sol. Energy Mater. Sol. Cells* **144**, 84–95 (2018).
11. Ramanujam, J. et al. Flexible CIGS, CdTe and a-Si:H based thin film solar cells: a review. *Prog. Mater. Sci.* **110**, 100619 (2020).
12. Fukuda, K., Yu, K. & Someya, T. The future of flexible organic solar cells. *Adv. Energy Mater.* **10**, 2000765 (2020).
13. Cheng, P. & Zhan, X. Stability of organic solar cells: challenges and strategies. *Chem. Soc. Rev.* **45**, 2544–2582 (2016).
14. Duan, L. & Uddin, A. Progress in stability of organic solar cells. *Adv. Sci.* **7**, 1903259 (2020).
15. Giraldo, S. et al. Progress and perspectives of thin film kesterite photovoltaic technology: a critical review. *Adv. Mater.* **31**, e1806692 (2019).
16. Walsh, A., Chen, S., Wei, S.-H. & Gong, X.-G. Kesterite thin-film solar cells: advances in materials modelling of $\text{Cu}_2\text{ZnSnS}_4$. *Adv. Energy Mater.* **2**, 400–409 (2012).
17. Li, J., Wang, D., Li, X., Zeng, Y. & Zhang, Y. Cation substitution in earth-abundant kesterite photovoltaic materials. *Adv. Sci.* **5**, 1700744 (2018).

18. Larramona, G. et al. Stability, reliability, upscaling and possible technological applications of kesterite solar cells. *J. Phys. Energy* **2**, 024009 (2020).
19. Wang, A. et al. Analysis of manufacturing cost and market niches for $\text{Cu}_2\text{ZnSnS}_4$ (CZTS) solar cells. *Sustain. Energy Fuels* **5**, 1044–1058 (2021).
20. Yamaguchi, M. et al. Analysis for efficiency potential of II–VI compound, chalcopyrite, and kesterite-based tandem solar cells. *J. Mater. Res.* **37**, 445–456 (2022).
21. Ho-Baillie, A. W. Y. et al. Recent progress and future prospects of perovskite tandem solar cells. *Appl. Phys. Rev.* **8**, 041307 (2021).
22. Li, K. et al. Fabrication and optimization of CdSe solar cells for possible top cell of silicon-based tandem devices. *Adv. Energy Mater.* **12**, 2200725 (2022).
23. Meillaud, F., Shah, A., Droz, C., Vallat-Sauvain, E. & Miazza, C. Efficiency limits for single-junction and tandem solar cells. *Sol. Energy Mater. Sol. Cells* **90**, 2952–2959 (2006).
24. De Vos, A. Detailed balance limit of the efficiency of tandem solar cells. *J. Phys. D Appl. Phys.* **13**, 839 (1980).
25. He, M. et al. Kesterite solar cells: insights into current strategies and challenges. *Adv. Sci.* **8**, 2004313 (2021).
26. Kim, S., Márquez, J. A., Unold, T. & Walsh, A. Upper limit to the photovoltaic efficiency of imperfect crystals from first principles. *Energy Environ. Sci.* **13**, 1481–1491 (2020).
27. Li, J. et al. Unveiling microscopic carrier loss mechanisms in 12% efficient $\text{Cu}_2\text{ZnSnSe}_4$ solar cells. *Nat. Energy* **7**, 754–764 (2022).
28. Mitzi, D. B., Gunawan, O., Todorov, T. K., Wang, K. & Guha, S. The path towards a high-performance solution-processed kesterite solar cell. *Sol. Energy Mater. Sol. Cells* **95**, 1421–1436 (2011).
29. Li, J. et al. Interface recombination of $\text{Cu}_2\text{ZnSnS}_4$ solar cells leveraged by high carrier density and interface defects. *Sol. RRL* **5**, 2100418 (2021).
30. Wang, W. et al. Device characteristics of CZTSSe thin-film solar cells with 12.6% efficiency. *Adv. Energy Mater.* **4**, 1301465 (2014).
31. Todorov, T. K. et al. Beyond 11% efficiency: characteristics of state-of-the-art $\text{Cu}_2\text{ZnSn(S,Se)}_4$ solar cells. *Adv. Energy Mater.* **3**, 34–38 (2013).
32. Fritsche, J., Klein, A. & Jaegermann, W. Thin film solar cells: materials science at interfaces. *Adv. Eng. Mater.* **7**, 914–920 (2005).
33. He, M., Sun, K., Suryawanshi, M. P., Li, J. & Hao, X. Interface engineering of p-n heterojunction for kesterite photovoltaics: a progress review. *J. Energy Chem.* **60**, 1–8 (2021).
34. Mellikov, E. et al. in *Copper Zinc Tin Sulfide-Based Thin-Film Solar Cells* (ed. Ito, K.) 289–309 (Wiley, 2014).
35. Son, D.-H. et al. Effect of solid-H₂S gas reactions on CZTSSe thin film growth and photovoltaic properties of a 12.62% efficiency device. *J. Mater. Chem. A* **7**, 25279–25289 (2019).
36. Li, J. et al. Defect control for 12.5% efficiency $\text{Cu}_2\text{ZnSnSe}_4$ kesterite thin-film solar cells by engineering of local chemical environment. *Adv. Mater.* **32**, 2005268 (2020).
37. Gong, Y. et al. Ag incorporation with controlled grain growth enables 12.5% efficient kesterite solar cell with open circuit voltage reached 64.2% Shockley–Queisser limit. *Adv. Funct. Mater.* **31**, 2101927 (2021).
38. Wang, J. et al. Ge bidirectional diffusion to simultaneously engineer back interface and bulk defects in the absorber for efficient CZTSSe solar cells. *Adv. Mater.* **34**, 2202858 (2022).
39. Yan, C. et al. $\text{Cu}_2\text{ZnSnS}_4$ solar cells with over 10% power conversion efficiency enabled by heterojunction heat treatment. *Nat. Energy* **3**, 764–772 (2018).
40. Giraldo, S. et al. How small amounts of Ge modify the formation pathways and crystallization of kesterites. *Energy Environ. Sci.* **11**, 582–593 (2018).
41. Scragg, J. J., Dale, P. J., Colombara, D. & Peter, L. M. Thermodynamic aspects of the synthesis of thin-film materials for solar cells. *Chemphyschem* **13**, 3035–3046 (2012).
42. Liu, F. et al. Nanoscale microstructure and chemistry of $\text{Cu}_2\text{ZnSnS}_4/\text{CdS}$ interface in kesterite $\text{Cu}_2\text{ZnSnS}_4$ solar cells. *Adv. Energy Mater.* **6**, 1600706 (2016).
43. Xu, B. et al. Positive role of inhibiting CZTSSe decomposition on intrinsic defects and interface recombination of 12.03% efficient kesterite solar cells. *Sol. RRL* **6**, 2200256 (2022).
44. Shin, D., Saparov, B. & Mitzi, D. B. Defect engineering in multinary earth-abundant chalcogenide photovoltaic materials. *Adv. Energy Mater.* **7**, 1602366 (2017).
45. Yin, K. et al. A high-efficiency (12.5%) kesterite solar cell realized by crystallization growth kinetics control over aqueous solution based $\text{Cu}_2\text{ZnSn(S,Se)}_4$. *J. Mater. Chem. A* **10**, 779–788 (2022).
46. Cui, Y. et al. DMF-based large-grain spanning $\text{Cu}_2\text{ZnSn(S}_x\text{Se}_{1-x})_4$ device with a PCE of 11.76. *Adv. Sci.* **9**, 2201241 (2022).
47. Fu, J. et al. Rational design of heterojunction interface for $\text{Cu}_2\text{ZnSn(S,Se)}_4$ solar cells to exceed 12% efficiency. *Sol. RRL* **6**, 2101032 (2022).
48. Sun, Y. et al. N-type surface design for p-type CZTSSe thin film to attain high efficiency. *Adv. Mater.* **33**, 2104330 (2021).
49. Cui, C. et al. Surface defect ordered $\text{Cu}_2\text{ZnSn(S,Se)}_4$ solar cells with efficiency over 12% via manipulating local substitution. *J. Energy Chem.* **67**, 555–562 (2022).
50. Taskesen, T. et al. Device characteristics of an 11.4% CZTSe solar cell fabricated from sputtered precursors. *Adv. Energy Mater.* **8**, 1703295 (2018).
51. Lee, Y. S. et al. $\text{Cu}_2\text{ZnSnSe}_4$ thin-film solar cells by thermal co-evaporation with 11.6% efficiency and improved minority carrier diffusion length. *Adv. Energy Mater.* **5**, 1401372 (2015).
52. Gang, M. G. et al. A facile process for partial Ag substitution in kesterite $\text{Cu}_2\text{ZnSn(S,Se)}_4$ solar cells enabling a device efficiency of over 12%. *ACS Appl. Mater. Interfaces* **13**, 3959–3968 (2021).
53. Kim, S., Kim, K. M., Tampo, H., Shibata, H. & Niki, S. Improvement of voltage deficit of Ge-incorporated kesterite solar cell with 12.3% conversion efficiency. *Appl. Phys. Express* **9**, 102301 (2016).
54. Tampo, H., Kim, S., Nagai, T., Shibata, H. & Niki, S. Improving the open circuit voltage through surface oxygen plasma treatment and 11.7% efficient $\text{Cu}_2\text{ZnSnSe}_4$ solar cell. *ACS Appl. Mater. Interfaces* **11**, 13319–13325 (2019).
55. Zhou, Z., Wang, Y., Xu, D. & Zhang, Y. Fabrication of $\text{Cu}_2\text{ZnSnS}_4$ screen printed layers for solar cells. *Sol. Energy Mater. Sol. Cells* **94**, 2042–2045 (2010).
56. Becerril-Romero, I. et al. CZTSe solar cells developed on polymer substrates: effects of low-temperature processing. *Prog. Photovolt. Res. Appl.* **26**, 55–68 (2018).
57. Bras, P., Sterner, J. & Platzer-Björkman, C. Influence of hydrogen sulfide annealing on copper–zinc–tin–sulfide solar cells sputtered from a quaternary compound target. *Thin Solid Films* **582**, 233–238 (2015).
58. López-Marino, S. et al. Earth-abundant absorber based solar cells onto low weight stainless steel substrate. *Sol. Energy Mater. Sol. Cells* **130**, 347–353 (2014).
59. López-Marino, S. et al. Alkali doping strategies for flexible and light-weight $\text{Cu}_2\text{ZnSnSe}_4$ solar cells. *J. Mater. Chem. A* **4**, 1895–1907 (2016).
60. Sun, K. et al. Flexible kesterite $\text{Cu}_2\text{ZnSnS}_4$ solar cells with sodium-doped molybdenum back contacts on stainless steel substrates. *Sol. Energy Mater. Sol. Cells* **182**, 14–20 (2018).
61. Peng, C.-Y. et al. Fabrication of $\text{Cu}_2\text{ZnSnS}_4$ solar cell on a flexible glass substrate. *Thin Solid Films* **562**, 574–577 (2014).
62. Brew, K. W., McLeod, S. M., Garner, S. M. & Agrawal, R. Improving efficiencies of $\text{Cu}_2\text{ZnSnS}_4$ nanoparticle based solar cells on flexible glass substrates. *Thin Solid Films* **642**, 110–116 (2017).
63. Sun, L., Shen, H., Huang, H., Raza, A. & Zhao, Q. Effect of evaporated Sb layer on performance of flexible CZTSSe thin film solar cell. *Sol. Energy* **193**, 267–274 (2019).
64. Sun, L. et al. Flexible CZTSSe thin film solar cells fabricated at low temperature with relieved residual stress by Sb incorporation. *Ceram. Int.* **46**, 1982–1989 (2020).
65. Zhao, Q. et al. Effect of sodium doping on crystal growth and band matching of the heterojunction in flexible CZTS solar cells. *J. Mater. Chem. C* **9**, 17531–17541 (2021).
66. Dong, L., Cheng, S., Lai, Y., Zhang, H. & Jia, H. Sol-gel processed CZTS thin film solar cell on flexible molybdenum foil. *Thin Solid Films* **626**, 168–172 (2017).
67. Yang, K. J. et al. Sodium effects on the diffusion, phase, and defect characteristics of kesterite solar cells and flexible $\text{Cu}_2\text{ZnSn(S,Se)}_4$ with greater than 11% efficiency. *Adv. Funct. Mater.* **31**, 2102238 (2021).
68. Xie, W. et al. 10.24% efficiency of flexible $\text{Cu}_2\text{ZnSn(S,Se)}_4$ solar cells by pre-evaporation selenization technique. *Small* **18**, 2201347 (2022).
69. Xu, H. et al. 9.63% efficient flexible $\text{Cu}_2\text{ZnSn(S,Se)}_4$ solar cells fabricated via scalable doctor-blading under ambient conditions. *J. Mater. Chem. A* **9**, 25062–25072 (2021).
70. Kim, S.-Y. et al. Void and secondary phase formation mechanisms of CZTSSe using Sn/Cu/Zn/Mo stacked elemental precursors. *Nano Energy* **59**, 399–411 (2019).
71. Yang, K. J. et al. Flexible $\text{Cu}_2\text{ZnSn(S,Se)}_4$ solar cells with over 10% efficiency and methods of enlarging the cell area. *Nat. Commun.* **10**, 2959 (2019).
72. Deng, H. et al. Novel symmetrical bifacial flexible CZTSSe thin film solar cells for indoor photovoltaic applications. *Nat. Commun.* **12**, 3107 (2021).
73. Todorov, T. et al. Flexible kesterite solar cells on ceramic substrates for advanced thermal processing. In *IEEE 42nd Photovoltaic Specialist Conference (PVSC)* 1–3 (IEEE, 2015).
74. Min, J. H. et al. Flexible high-efficiency CZTSSe solar cells on diverse flexible substrates via an adhesive-bonding transfer method. *ACS Appl. Mater. Interfaces* **12**, 8189–8197 (2020).
75. Peňar, G. et al. Challenges in the industrial production of CZTS monograin solar cells. In *IEEE 44th Photovoltaic Specialist Conference (PVSC)* 178–181 (IEEE, 2017).
76. Timmo, K. et al. The effect of Ag alloying of $\text{Cu}_2(\text{Zn,Cd})\text{SnS}_4$ on the monograin powder properties and solar cell performance. *J. Mater. Chem. A* **7**, 24281–24291 (2019).
77. Lloyd, M. A. et al. Effects of composition and thermal treatment on V_{OC} -limiting defects in single-crystalline $\text{Cu}_2\text{ZnSnSe}_4$ solar cells. *Prog. Photovolt. Res. Appl.* **30**, 503517 (2022).

78. Kauk-Kuusik, M. et al. Detailed insight into the CZTS/CdS interface modification by air annealing in monograin layer solar cells. *ACS Appl. Energy Mater.* **4**, 12374–12382 (2021).
79. Neubauer, C., Samiepour, A., Oueslati, S., Ernits, K. & Meissner, D. Spatially resolved opto-electrical performance investigations of $\text{Cu}_2\text{ZnSnS}_3\text{Se}_{0.8}$ photovoltaic devices. *Energy Sci. Eng.* **6**, 563–569 (2018).
80. Timmo, K. et al. Influence of order-disorder in $\text{Cu}_2\text{ZnSnS}_4$ powders on the performance of monograin layer solar cells. *Thin Solid Films* **633**, 122–126 (2017).
81. Kauk-Kuusik, M. et al. Reduced recombination through CZTS/CdS interface engineering in monograin layer solar cells. *J. Phys. Energy* **4**, 024007 (2022).
82. Gong, Y. et al. Identifying the origin of the Voc deficit of kesterite solar cells from the two grain growth mechanisms induced by Sn^{2+} and Sn^{4+} precursors in DMSO solution. *Energy Environ. Sci.* **14**, 2369–2380 (2021).
83. Wang, Y.-C., Wu, T.-T. & Chueh, Y.-L. A critical review on flexible $\text{Cu}(\text{In}, \text{Ga})\text{Se}_2$ (CIGS) solar cells. *Mater. Chem. Phys.* **234**, 329–344 (2019).
84. Zhu, H. et al. DC and RF sputtered molybdenum electrodes for $\text{Cu}(\text{In}, \text{Ga})\text{Se}_2$ thin film solar cells. *Appl. Surf. Sci.* **465**, 48–55 (2019).
85. Martinho, F. et al. Persistent double-layer formation in kesterite solar cells: a critical review. *ACS Appl. Mater. Interfaces* **12**, 39405–39424 (2020).
86. Li, J. et al. Large-grain spanning monolayer $\text{Cu}_2\text{ZnSnSe}_4$ thin-film solar cells grown from metal precursor. *Small* **18**, 2105044 (2022).
87. Yuan, Z.-K. et al. Engineering solar cell absorbers by exploring the band alignment and defect disparity: the case of Cu- and Ag-based kesterite compounds. *Adv. Funct. Mater.* **25**, 6733–6743 (2015).
88. Su, Z. et al. Cation substitution of solution-processed $\text{Cu}_2\text{ZnSnS}_4$ thin film solar cell with over 9% efficiency. *Adv. Energy Mater.* **5**, 1500682 (2015).
89. Chen, R. & Persson, C. Electronic and optical properties of Cu_2XSnS_4 (X = Be, Mg, Ca, Mn, Fe, and Ni) and the impact of native defect pairs. *J. Appl. Phys.* **121**, 203104 (2017).
90. Lie, S. et al. Comprehensive physicochemical and photovoltaic analysis of different Zn substitutes (Mn, Mg, Fe, Ni, Co, Ba, Sr) in CZTS-inspired thin film solar cells. *J. Mater. Chem. A* **10**, 9137–9149 (2022).
91. Zhang, J. et al. Enhancing electrical properties of $\text{Cu}_2\text{ZnSn}(\text{S}, \text{Se})_4$ thin films via trace Co incorporation. *Mater. Chem. Phys.* **262**, 124318 (2021).
92. Li, B. et al. Barrier effect of AlN film in flexible $\text{Cu}(\text{In}, \text{Ga})\text{Se}_2$ solar cells on stainless steel foil and solar cell. *J. Alloy. Compd.* **627**, 1–6 (2015).
93. Herz, K., Eicke, A., Kessler, F., Wächter, R. & Powalla, M. Diffusion barriers for CIGS solar cells on metallic substrates. *Thin Solid Films* **431**, 392–397 (2003).
94. Gershon, T. et al. The role of sodium as a surfactant and suppressor of non-radiative recombination at internal surfaces in $\text{Cu}_2\text{ZnSnS}_4$. *Adv. Energy Mater.* **5**, 1400849 (2015).
95. Shi, X. et al. Significantly improving the crystal growth of a $\text{Cu}_2\text{ZnSn}(\text{S}, \text{Se})_4$ absorber layer by air-annealing a $\text{Cu}_2\text{ZnSnS}_4$ precursor thin film. *ACS Appl. Mater. Interfaces* **12**, 41590–41595 (2020).
96. Tampo, H., Kim, K. M., Kim, S., Shibata, H. & Niki, S. Improvement of minority carrier lifetime and conversion efficiency by Na incorporation in $\text{Cu}_2\text{ZnSnSe}_4$ solar cells. *J. Appl. Phys.* **122**, 023106 (2017).
97. Xin, H. et al. Lithium-doping inverts the nanoscale electric field at the grain boundaries in $\text{Cu}_2\text{ZnSn}(\text{S}, \text{Se})_4$ and increases photovoltaic efficiency. *Phys. Chem. Chem. Phys.* **17**, 23859–23866 (2015).
98. He, M. et al. High efficiency $\text{Cu}_2\text{ZnSn}(\text{S}, \text{Se})_4$ solar cells with shallow LiZn acceptor defects enabled by solution-based Li post-deposition treatment. *Adv. Energy Mater.* **11**, 2003783 (2021).
99. Zhou, H. et al. Rational defect passivation of $\text{Cu}_2\text{ZnSn}(\text{S}, \text{Se})_4$ photovoltaics with solution-processed $\text{Cu}_2\text{ZnSnS}_4$:Na nanocrystals. *J. Am. Chem. Soc.* **135**, 15998–16001 (2013).
100. Sun, K. et al. Influence of sodium incorporation on kesterite $\text{Cu}_2\text{ZnSnS}_4$ solar cells fabricated on stainless steel substrates. *Sol. Energy Mater. Sol. Cells* **157**, 565–571 (2016).
101. Bär, M. et al. Cliff-like conduction band offset and KCN-induced recombination barrier enhancement at the $\text{CdS}/\text{Cu}_2\text{ZnSnS}_4$ thin-film solar cell heterojunction. *Appl. Phys. Lett.* **99**, 222105 (2011).
102. Just, J., Lützenkirchen-Hecht, D., Frahm, R., Schorr, S. & Unold, T. Determination of secondary phases in kesterite $\text{Cu}_2\text{ZnSnS}_4$ thin films by x-ray absorption near edge structure analysis. *Appl. Phys. Lett.* **99**, 262105 (2011).
103. Just, J., Lützenkirchen-Hecht, D., Müller, O., Frahm, R. & Unold, T. Depth distribution of secondary phases in kesterite $\text{Cu}_2\text{ZnSnS}_4$ by angle-resolved X-ray absorption spectroscopy. *APL Mater.* **5**, 126106 (2017).
104. Bär, M. et al. CdS/low-band-gap kesterite thin-film solar cell absorber heterojunction: energy level alignment and dominant recombination process. *ACS Appl. Energy Mater.* **1**, 475–482 (2018).
105. Bär, M. et al. Electronic structure of $\text{Cu}_2\text{ZnSnS}_4$ probed by soft x-ray emission and absorption spectroscopy. *Phys. Rev. B* **84**, 035308 (2011).
106. Kim, S., Park, J.-S., Hood, S. N. & Walsh, A. Lone-pair effect on carrier capture in $\text{Cu}_2\text{ZnSnS}_4$ solar cells. *J. Mater. Chem. A* **7**, 2686–2693 (2019).
107. Li, J., Yuan, Z.-K., Chen, S., Gong, X.-G. & Wei, S.-H. Effective and noneffective recombination center defects in $\text{Cu}_2\text{ZnSnS}_4$: significant difference in carrier capture cross sections. *Chem. Mater.* **31**, 826–833 (2019).
108. Park, J. S., Kim, S., Xie, Z. & Walsh, A. Point defect engineering in thin-film solar cells. *Nat. Rev. Mater.* **3**, 194–210 (2018).
109. Romanyuk, Y. E. et al. Doping and alloying of kesterites. *J. Phys. Energy* **1**, 044004 (2019).
110. Hages, C. J. et al. Identifying the real minority carrier lifetime in nonideal semiconductors: a case study of kesterite materials. *Adv. Energy Mater.* **7**, 1700167 (2017).
111. Platzer-Björkman, C. et al. Back and front contacts in kesterite solar cells: state-of-the-art and open questions. *J. Phys. Energy* **1**, 044005 (2019).
112. Park, H. K. et al. Flexible kesterite thin-film solar cells under stress. *npj Flex. Electron.* **6**, 91 (2022).
113. NREL. Best research-cell efficiency chart, regularly updated by NREL. <https://www.nrel.gov/pv/cell-efficiency.html> (2023).
114. Green, M. A. et al. Solar cell efficiency tables (version 60). *Prog. Photovolt. Res. Appl.* **30**, 687–701 (2022).
115. Tian, Q. et al. Hydrophilic $\text{Cu}_2\text{ZnSnS}_4$ nanocrystals for printing flexible, low-cost and environmentally friendly solar cells. *CrystEngComm* **14**, 3847 (2012).
116. Yu, X. et al. Efficient $(\text{Cu}_{1-x}\text{Ag}_x)_2\text{ZnSn}(\text{S}, \text{Se})_4$ solar cells on flexible Mo foils. *RSC Adv.* **8**, 27686–27694 (2018).
117. Jo, E. et al. 8% Efficiency $\text{Cu}_2\text{ZnSn}(\text{S}, \text{Se})_4$ (CZTSSe) thin film solar cells on flexible and lightweight molybdenum foil substrates. *ACS Appl. Mater. Interfaces* **11**, 23118–23124 (2019).
118. Yan, Q. et al. High flexible $\text{Cu}_2\text{ZnSn}(\text{S}, \text{Se})_4$ solar cells by green solution-process. *Sol. Energy* **177**, 508–516 (2019).
119. Yu, X. et al. Efficient flexible Mo foil-based $\text{Cu}_2\text{ZnSn}(\text{S}, \text{Se})_4$ solar cells from In-doping technique. *Sol. Energy Mater. Sol. Cells* **209**, 110434 (2020).
120. Ge, S. et al. A universal and facile method of tailoring the thickness of $\text{Mo}(\text{S}_{x-1}\text{Se}_{1-x})_2$, contributing to highly efficient flexible $\text{Cu}_2\text{ZnSn}(\text{S}, \text{Se})_4$ solar cells. *Sol. RRL* **5**, 2100598 (2021).
121. Liu, J. et al. In situ electrochemical treatment evoked superior grain growth for green electrodeposition-processed flexible CZTSe solar cells. *ACS Appl. Mater. Interfaces* **13**, 31852–31860 (2021).
122. Park, H. K. et al. Chemical tailoring of sodium content for optimization of interfacial band bending and alignment in flexible kesterite solar cells. *Sol. Energy Mater. Sol. Cells* **230**, 111243 (2021).
123. Sun, Q. et al. Efficiency improvement of flexible $\text{Cu}_2\text{ZnSn}(\text{S}, \text{Se})_4$ solar cells by window layer interface engineering. *ACS Appl. Energy Mater.* **4**, 14467–14475 (2021).
124. Gang, M. G. et al. Band tail engineering in kesterite $\text{Cu}_2\text{ZnSn}(\text{S}, \text{Se})_4$ thin-film solar cells with 11.8% efficiency. *J. Phys. Chem. Lett.* **9**, 4555–4561 (2018).
125. Su, Z. et al. Device postannealing enabling over 12% efficient solution-processed $\text{Cu}_2\text{ZnSnS}_4$ solar cells with $\text{Cd}(2+)$ substitution. *Adv. Mater.* **32**, 2000121 (2020).
126. Schorr, S. & Gonzalez-Aviles, G. In-situ investigation of the structural phase transition in kesterite. *Phys. Status Solidi (A)* **206**, 1054–1058 (2009).
127. Stanchik, A. V., Chumak, V., Gremenok, V. F., Baraishuk, S. M. & Shoukavaya, T. A low-temperature X-ray diffraction study of the $\text{Cu}_2\text{ZnSnSe}_4$ thin films on a mo foil substrate. In *37th European Photovoltaic Solar Energy Conference and Exhibition 722–724* (Fraunhofer Institute for Solar Energy Systems, 2020).
128. El-Mahalawy, S. H. & Evans, B. L. The thermal expansion of ${}^2\text{H-MoSe}_2$, ${}^2\text{H-MoSe}_2$ and ${}^2\text{H-WSe}_2$ between 20 and 800 C. *J. Appl. Crystallogr.* **9**, 403–406 (1976).
129. Kumar, D., Kumar, V., Kumar, R., Kumar, M. & Kumar, P. Electron-phonon coupling, thermal expansion coefficient, resonance effect, and phonon dynamics in high-quality CVD-grown monolayer and bilayer MoSe_2 . *Phys. Rev. B* **105**, 085419 (2022).

ACKNOWLEDGEMENTS

J.L., K.S. J.H., X.H., and M.A.G. acknowledge the financial support of the Australian government through the Australian Renewable Energy Agency (ARENA) (grant number 2017/RND006), Baosteel (grant number LP150100911). X.H. acknowledges the financial support of the Australian Research Council (ARC) Future Fellowship (FT190100756). J.L. and K.S. acknowledges the support from Australian Centre of Advanced Photovoltaics (ACAP, RG200768-A and RG172864-B, respectively). Responsibility for the views, information, or advice expressed herein is not accepted by the Australian government.

AUTHOR CONTRIBUTIONS

J.L. drafted and revised the manuscript. K.S. drafted the “Na incorporation” section. X.Y. and J.H. assisted in visualization. X.H. and M.A.G. supervised the manuscript. All authors discussed and commented on the manuscript.

COMPETING INTERESTS

The authors declare no competing interests.

ADDITIONAL INFORMATION

Correspondence and requests for materials should be addressed to Jianjun Li, Kaiwen Sun or Xiaojing Hao.

Reprints and permission information is available at <http://www.nature.com/reprints>

Publisher's note Springer Nature remains neutral with regard to jurisdictional claims in published maps and institutional affiliations.



Open Access This article is licensed under a Creative Commons Attribution 4.0 International License, which permits use, sharing, adaptation, distribution and reproduction in any medium or format, as long as you give appropriate credit to the original author(s) and the source, provide a link to the Creative Commons license, and indicate if changes were made. The images or other third party material in this article are included in the article's Creative Commons license, unless indicated otherwise in a credit line to the material. If material is not included in the article's Creative Commons license and your intended use is not permitted by statutory regulation or exceeds the permitted use, you will need to obtain permission directly from the copyright holder. To view a copy of this license, visit <http://creativecommons.org/licenses/by/4.0/>.

© The Author(s) 2023